Applied Catalysis B: Environmental 334 (2023) 122811

Contents lists available at ScienceDirect

Applied Catalysis B: Environmental

journal homepage: www.elsevier.com/locate/apcatb

New insights into the catalytic mechanism of VOCs abatement over Pt/Beta with active sites regulated by zeolite acidity

Daiqiang Li [a,b], Lian Wang [a,b,*], Yuqin Lu [b,c], Hua Deng [b,c,**], Zhilin Zhang [a,b], Yingjie Wang [a,b], Ying Ma [d], Tingting Pan [b,c], Qian Zhao [a], Yulong Shan [a], Xiaoyan Shi [a,b], Jinzhu Ma [a,b], Hong He [a,b,c]

[a] State Key Joint Laboratory of Environment Simulation and Pollution Control, Research Center for Eco-Environmental Sciences, Chinese Academy of Sciences, Beijing 100085, China
[b] University of Chinese Academy of Sciences, Beijing 100049, China
[c] Center for Excellence in Regional Atmospheric Environment, Institute of Urban Environment, Chinese Academy of Sciences, Xiamen 361021, China
[d] Department of Chemical Engineering, Hebei Petroleum University of Technology, Chengde 067000, China

ARTICLE INFO

Keywords:
Beta zeolite-supported Pt
Active site regulation
Si/Al ratio
Brønsted acid sites
VOC oxidation mechanism
DFT calculations

ABSTRACT

Zeolite-supported noble metal catalysts have good low-temperature activity and efficacy in eliminating VOCs contaminants. Regulating the nature of active sites is beneficial for improving the catalytic oxidation performance and decreasing coke deposition for further increase in the durability. In this work, Pt/Beta catalysts for toluene oxidation with different valence states, location, and dispersion of Pt were achieved through regulation of active sites using the acidity of zeolites with different Si/Al ratios. It was revealed that $Pt^{\delta+}$ were highly dispersed on the low Si/Al ratio of 6 including isolated $Z[Pt^{2+}(OH)]^+$ originated from Pt^{2+} ions anchored on ion-exchange sites (strong Brønsted acid sites) of Beta zeolites, while Pt^0 nanoparticles were the main active sites of Beta zeolites with the high Si/Al ratio of 260 without H_2 post-treatment. The Pt/Beta catalysts with high silica had better catalytic oxidation performance than that with low silica because Pt^0 had stronger activation ability towards O_2 as well as more facile oxygen replenishment than $Pt^{\delta+}$. It was noted that the key role of OH groups led to the enhanced oxidation of toluene driven by water vapor. Both high-silica and low-silica Pt/Beta catalysts exhibited excellent durability for 60 h of operation with no detectable decrease in catalytic performance and followed similar toluene oxidation pathways, forming intermediates including alkoxides, carboxylates, and anhydrides. The difference was that the quantity of gaseous benzene generated on high-silica Pt/Beta was much lower than that on low-silica Pt/Beta, indicating that Pt^0 rather than $Pt^{\delta+}$ was conducive to the benzene ring opening reaction. The strong ability of Pt^0 to activate O_2 and the reduction of $Pt^{\delta+}$ into Pt^0 during the reaction process could be responsible for the excellent durability and similar reaction pathways towards both low-silica and high-silica Pt/Beta. This study provides guidance for the regulation of active sites and design of efficient zeolite-based catalysts for VOCs abatement.

1. Introduction

Volatile organic compounds (VOCs) are mainly emitted from decorative materials, solvent utilization, automobile exhaust and industrial production [1,2]. Due to the wide variety of VOCs sources, they can contribute to both indoor and outdoor pollution and cause damage to the atmospheric environment and human health [3]. Within VOCs, BTX (benzene, toluene, xylene) are major pollutants with strong carcinogenicity and blood toxicity as well as being precursor substances contributing to ozone and photochemical pollution [4,5]. The elimination technologies used for VOCs mainly include recovery and destruction technologies, such as adsorption, catalytic oxidation, thermal incineration, ozone-catalysis, plasma-catalysis, etc. [6–8]. In particular, the catalytic oxidation technologies are currently considered as among the

* Corresponding author at: State Key Joint Laboratory of Environment Simulation and Pollution Control, Research Center for Eco-Environmental Sciences, Chinese Academy of Sciences, Beijing 100085, China.
** Corresponding author at: University of Chinese Academy of Sciences, Beijing 100049, China.
E-mail addresses: lianwang@rcees.ac.cn (L. Wang), huadeng@iue.ac.cn (H. Deng).

https://doi.org/10.1016/j.apcatb.2023.122811
Received 30 November 2022; Received in revised form 8 April 2023; Accepted 24 April 2023
Available online 26 April 2023

most efficient methods to remove VOCs, and can realize complete oxidation at relatively low temperatures to degrade VOCs with no secondary pollutants [9,10]. Compared with transition metal oxide catalysts, noble metal catalysts have better low-temperature activity and durability [11,12].

Zeolites show excellent performance in the adsorption of VOCs due to their high specific surface area and numerous parameters that can be adjusted, including acid sites and pore structure, giving them advantages as catalyst supports [12–14]. In order to improve their oxidation ability and durability, zeolite-supported noble metal catalysts have been well-developed to provide sufficient adsorption and oxidation sites towards VOCs abatement. The current research on zeolites is mainly focused on ZSM-5 and BEA [15–18]. It was reported that the Pt loaded on pore-modified ZSM-5 foam could achieve almost complete catalytic oxidation of toluene at about 160 °C [15]. Chen et al. found that Pt/ZSM-5 catalysts with a platinum particle mean diameter of 1.9 nm could achieve complete catalytic oxidation of toluene at about 155 °C [16]. Aluminum-rich Beta zeolite-supported Pt catalysts exhibited significantly increased catalytic ability and could completely oxidize toluene at 148 °C [17]. However, catalysts with excellent catalytic performance usually require post-treatment by H_2 reduction to form Pt^0 active sites with high oxidation ability [15–17]. H_2 post-treatment is hazardous and high-cost. Furthermore, zeolites with low oxidation ability are typically deactivated due to coke accumulation. Shi et al. showed that Pt loading could improve the redox ability of catalysts, thereby significantly improving their resistance to carbon deposition [19]. Some researchers mentioned that increasing the oxygen supply capacity of the catalysts could effectively reduce the amount of carbon deposition on the catalysts [20]. Researchers also proposed that the Si/Al ratio affected the dispersion of precious metals, resulting in an increase in the rate of catalytic oxidation of VOCs, which will also effectively reduce carbon deposits [21]. Therefore, it is very beneficial to be able to regulate the nature of active sites to improve catalytic oxidation performance and decrease coke deposition through a one-step method without post-treatment by a reductant such as H_2.

According to previous research in the literature, the Si/Al ratio and acidity of a zeolite can affect the nature of active sites. The results of Petrov and coworkers showed that the mobility of palladium on Pd/Na-MOR was inhibited by fully exchanging the acid sites of the zeolite with sodium, which kept palladium highly dispersed and prevented steam-induced sintering under reaction conditions [22]. Samad et al. also proved that aluminum-rich supports with more acidic sites were beneficial to achieving good Pt dispersion [23]. These results suggest that the dispersion of noble metals in zeolites can be influenced by the zeolite properties, such as the Si/Al ratio and acidity. Moreover, the acid-base properties of a zeolite also have an important impact on their hydrophobicity and adsorption properties. Our previous work revealed through experimental and theoretical research that the affinity between water vapor and zeolite or between VOCs and zeolite could be effectively reduced with an increase in the Si/Al ratio [13]. Previous reports also proposed that zeolites with high Si/Al ratios were more efficient for the adsorption and catalytic oxidation of toluene in humid air [24,25]. Further, the pore diameter of zeolite molecular sieves can affect the diffusion and adsorption of reactants and products, and it is generally believed that zeolite molecular sieves with pores having dynamic diameters similar to those of the reactants will be more conducive to oxidation reactions [26,27]. Therefore, the Beta zeolites (5.95–6.68 Å) with dynamic pore diameters similar to the size of a toluene molecule (6–7 Å) and different Si/Al ratios were selected as the supports in this work [28].

Herein, we report the preparation of Pt/Beta catalysts for toluene oxidation with different types of Pt species through regulating the acid sites of the Beta supports. The effects of the acid sites on the location, valence states, dispersion, and redox capacity of active sites on Pt/Beta catalysts as well as the catalytic oxidation performance, durability, water effect and activation ability towards toluene and oxygen were revealed via designed experiments combined with density functional theory (DFT) calculations. A mechanism for the performance differences of Pt/Beta catalysts with distinct active sites in the catalytic oxidation of toluene was finally proposed.

2. Experimental

2.1. Catalyst preparation

The catalysts were prepared by the traditional impregnation method. First, commercial Beta zeolites with different Si/Al ratios (Si/Al ratio = 6, 25, 260) were calcined at 600 °C for 3 h to obtain the final supports. The calcined Beta zeolites with different Si/Al ratios were mixed with appropriate amounts of $Pt(NH_3)_4(NO_3)_2$ solution and stirred for 2 h. Afterwards, the slurries were evaporated to complete dryness in a rotary evaporator under vacuum, then calcined at 550 °C for 3 h to obtain the Pt/Beta catalysts. The actual Si/Al ratios and Pt loadings of the Pt/Beta catalysts were measured by ICP-OES (Table 1). After Pt loading, the Si/Al ratios of Beta zeolites were essentially unchanged, and all catalysts had similar Pt contents of around 1 wt%. The samples were named Pt/Beta-6, Pt/Beta-25 and Pt/Beta-260 according to the Si/Al ratios of the supports. As a comparison, $Pt(NO_3)_2$ was used as an alternative source of Pt to prepare Pt/Beta catalysts with the same preparation process as described above except for the source of Pt; the obtained catalysts were named Pt/Beta-260-N when Beta with the Si/Al ratio of 260 was used. All used samples after toluene oxidation reaction were denoted as Pt/Beta-U.

2.2. Catalyst characterization

The Si, Al, and Pt contents of all samples were determined by Inductively Coupled Plasma Optical Emission Spectrometry (ICP-OES, OPTIMA 8300, PerkinElmer).

N_2 adsorption-desorption analysis was carried out on an ASAP 2460 Surface Area and Porosity System from Micromeritics, USA. Before testing, the samples were degassed at 300 °C for 6 h under vacuum to eliminate surface adsorbed impurities. The surface area, average pore width, micropore surface area and micropore volume, and mesoporous volume of the samples were obtained by the Brunauer-Emmett-Teller (BET), and nonlocal density functional theory (NLDFT), t-plot, and Barrett-Joyner-Halenda (BJH) methods, respectively.

X-ray diffraction (XRD) experiments for all powder samples were performed on a Bruker D8 Advance diffractometer with Cu Kα radiation (λ = 0.15406 nm), scan range (2θ) from 5° to 90° with step size of 0.02 s

The morphological characteristics and dispersion of all samples were investigated by Field Emission Scanning Electron Microscopy (FESEM) conducted with an SU-8020 Hitachi microscope with 15 kV acceleration voltage and 50× magnification. EDX elemental mappings were also performed at the same time.

X-ray adsorption fine structure (XAFS) spectra of samples were measured at room temperature in fluorescence mode on the 1W1B-XAFS experimental station in Beijing Synchrotron Radiation Facility (BSRF). Pt foil and PtO_2 were used as reference samples.

The adsorption performance for CO and toluene as well as the toluene oxidation mechanism of catalysts were investigated by *in situ* diffuse reflection infrared Fourier transform spectroscopy (DRIFTS) carried out on a Nicolet iS50 spectrometer with an MCT/A detector. All spectra were recorded from 4000 to 800 cm^{-1} with an accumulation of 90 scans at a resolution of 4 cm^{-1}. Before experiments, a background spectrum was collected under N_2 purge at the corresponding experimental temperature and later subtracted.

FTIR spectra of all Beta zeolites supports and Pt/Beta catalysts were carried out on a Nicolet iS50 spectrometer. The sample (30 mg) was pressed into thin sheets at a pressure of 5–6 MPa and placed in a vacuum chamber. Samples were first pretreated at 500 °C for 1 h in a vacuum to remove moisture, and then samples were cooled down to 120 °C to

Table 1
Structural parameters, Pt loading, and Si/Al ratios of Beta supports and Pt/Beta catalysts.

Sample	S_{BET} (m^2/g)	Average pore width (Å)	S_{Mic} (m^2/g)	Micropore volume (cm^3/g)	Mesoporous volume (cm^3/g)	Pt loading (wt%)	Si/Al ratios
Beta-6	481.5	7.7	367.3	0.19	0.32	/	6.4
Pt/Beta-6	433.7	8.1	332.9	0.17	0.32	0.94	6.7
Beta-25	471.7	7.9	363.3	0.19	0.19	/	24.8
Pt/Beta-25	454.7	8.0	351.6	0.18	0.20	0.97	21.6
Beta-260	545.5	8.1	401.4	0.21	0.19	/	258.6
Pt/Beta-260	530.9	8.5	391.6	0.20	0.18	0.92	255.2

record the spectra in a vacuum. All spectra were recorded from 4000 to 800 cm^{-1} with an accumulation of 90 scans at a resolution of 4 cm^{-1}.

H_2-temperature programmed reaction (H_2-TPR), Toluene-temperature programmed desorption-mass spectrometry (Toluene-TPD-MS) and Toluene-temperature programmed surface reaction-mass spectrometry (Toluene-TPSR-MS) were measured by an AutoChem II 2920 instrument from Micromeritics, USA. The signals were detected with a TCD detector equipped with the instrument or by mass spectrometry (MKS-Cirrus 2, USA) to monitor mass/charge ratio signals. Before the experiments, all of the samples were pretreated at 200 °C for one hour in 10 vol% O_2/He gas flow. For H_2-TPR, all samples were purged with Ar gas flow for one hour at room temperature, and then the samples were heated from 30 °C to 800 °C (ramp rate: 10 °C min^{-1}) in H_2/Ar gas flow. For Toluene-TPD-MS, all samples were treated with 2000 ppm toluene in 20 vol% O_2/N_2 for 3 h at room temperature. After reaching saturated adsorption, the samples were desorbed in He gas flow from 30 °C to 800 °C with a ramp of 10 °C min^{-1}. For Toluene-TPSR-MS, all samples were also treated with 2000 ppm toluene in 20 vol% O_2/N_2 for 3 h at room temperature. Then all samples were heated from 30 °C to 800 °C (ramp rate: 10 °C min^{-1}) in a 5 vol% $^{18}O_2$ gas flow.

The acidity and acid sites of samples were examined using NH_3 temperature programmed desorption (NH_3-TPD) measurements performed on the FTIR (Nicolet 380) with DTGS detector and 0.5 cm^{-1} resolution. Around 60 mg of sample was used and pretreated at 300 °C in 20 vol% O_2/N_2 for 30 min, then cooled to 120 °C followed by N_2 purging for 1 h. Then NH_3 adsorption was carried out under a gas flow of 500 ppm NH_3/N_2 at 120 °C until saturated. After that, the NH_3 flow was turned off and the sample was purged in N_2 for 1 h until the NH_3 signal was undetectable. The NH_3 desorption process was conducted from 120° to 600 °C with a ramp of 10 °C min^{-1}.

The ^{27}Al MAS NMR and ^{29}Si MAS NMR spectra of all samples were collected on a JNM-ECZ600R spectrometer, which was operated at a resonant frequency of 156 MHz (Al) or 119 MHz (Si) using a 3.2 mm MAS probe and relaxation delay of 5 s at room temperature. $AlCl_3$ and tetramethyl silane were used as external references, respectively.

2.3. Catalytic testing

In this study, the Pt/Beta catalysts with size 40–60 mesh were tested for toluene oxidation in a fixed-bed continuous flow reactor under atmospheric pressure. The reaction gas mixture was 200 ppm toluene in 80 vol% N_2 and 20 vol% O_2 with a flow of 50 mL/min, equivalent to a gas hourly space velocity (GHSV) of 20000 h^{-1}. The testing temperatures ranged from 100 °C to 200 °C, with monitoring conducted at 10 °C intervals, allowing two hours at each monitoring point to reach stability. The outlet concentrations of toluene and products were determined online using an Agilent 6890 N Gas Chromatograph equipped with TCD and FID detectors.

2.4. Calculation methodology

The DFT implementation in CP2K/Quickstep was performed using a hybrid Gaussian plane wave scheme to elucidate the activated configurations of toluene and oxygen in the pores of Pt/Beta catalysts [29]. The Gaussian basis set was DZVP, and the plane wave cutoff was set to 550 Ry. An orbital transformation method was used for wave function optimization with SCF convergence of 1×10^{-6} Hartree. The 5 s, 5p, 5d, 6 s electrons of Pt, 3p electrons of Al and Si 2 s, 2p electrons of O and C were treated as valence, and the remaining core electrons were described by GTH pseudopotentials [30]. The exchange-correlation functional was treated by using the PBE functional with the Grimme D3 method [31]. The geometries were optimized by the BFGS algorithm. The crystal cell lattice parameters for the high-silica BEA ($Si_{256}O_{512}$) and low-silica BEA ($H_{36}Al_{36}Si_{220}O_{512}$) zeolite used are listed in Table S1. A cubic nano-particle of Pt_{13} with size of about 0.5 nm was used to simulate the noble metal particles and a Pt^{2+} cluster was applied to model the highly dispersed single-atom sites. The isolated adsorbates (C_7H_8, O_2) were optimized in a 20 × 20 × 20 Å cubic cell. The adsorption energies of the adsorbates in the vicinity of Pt sites anchored in the micropores of BEA zeolites were calculated as follows:

$$E_a = E_{adsorbate+Pt/BEA} - \left(E_{Pt/BEA} + E_{adsorbate}\right)$$

Negative Ea values indicate that the adsorbed state is energetically favorable. In order to learn the charge transfer during adsorption, the calculation of charge density difference was also conducted.

3. Results and discussion

3.1. Catalytic performance

Toluene conversion and CO_2 generation as a function of temperature over the Pt/Beta catalysts with different Si/Al ratios are shown in Fig. 1 (a). More than 90% of the final products of the catalytic oxidation of toluene were CO_2 and H_2O, so the selectivity of CO_2 could precisely reflect the performance for the catalytic oxidation of toluene. It was demonstrated that Pt/Beta-260 had the best catalytic oxidation ability toward toluene and could completely oxidize toluene to CO_2 at about 160 °C. Previous report showed that H_2-reduced Pt/Beta catalysts with small size Pt^0 about 2 nm had the T_{98} of 189 °C for toluene oxidation at the same space velocity of 30,000 mL/g·h [32]. With the decrease in Si/Al ratio, the catalytic oxidation ability gradually decreased and the T_{90} of toluene conversion for Pt/Beta-25 was around 170 °C. In the case of Pt/Beta-6, the lowest oxidation ability was observed and the T_{90} was about 190 °C. In addition, Pt/Beta-6 had the optimal adsorption performance for toluene.

The catalytic activity results illustrated that Pt supported on Beta zeolites with high silica was more favorable for the catalytic oxidation of toluene. The stability test curves of Pt/Beta-6 and Pt/Beta-260 were measured at the same toluene conversion of around T_{50} (Fig. 1(b) and (c)) and T_{90} (Fig. S1) for approximately 60 h. It was worth noting that the conversion of toluene and the CO_2 generation remained stable over this long period at both T_{50} and T_{90}, which indicated that the catalysts had excellent durability and no clear carbon deposition, thus good potential for application. Generally, strong Brønsted acid sites were the active centers of carbon deposition formation, and carbon deposition covering the strong Brønsted acid sites led to inactivation of the catalysts [21,33]. The unique excellent characteristics such as high dispersion of active sites and excellent ability to activate oxygen at both high silica and low silica as well as the lack of acidic sites in the case of high silica

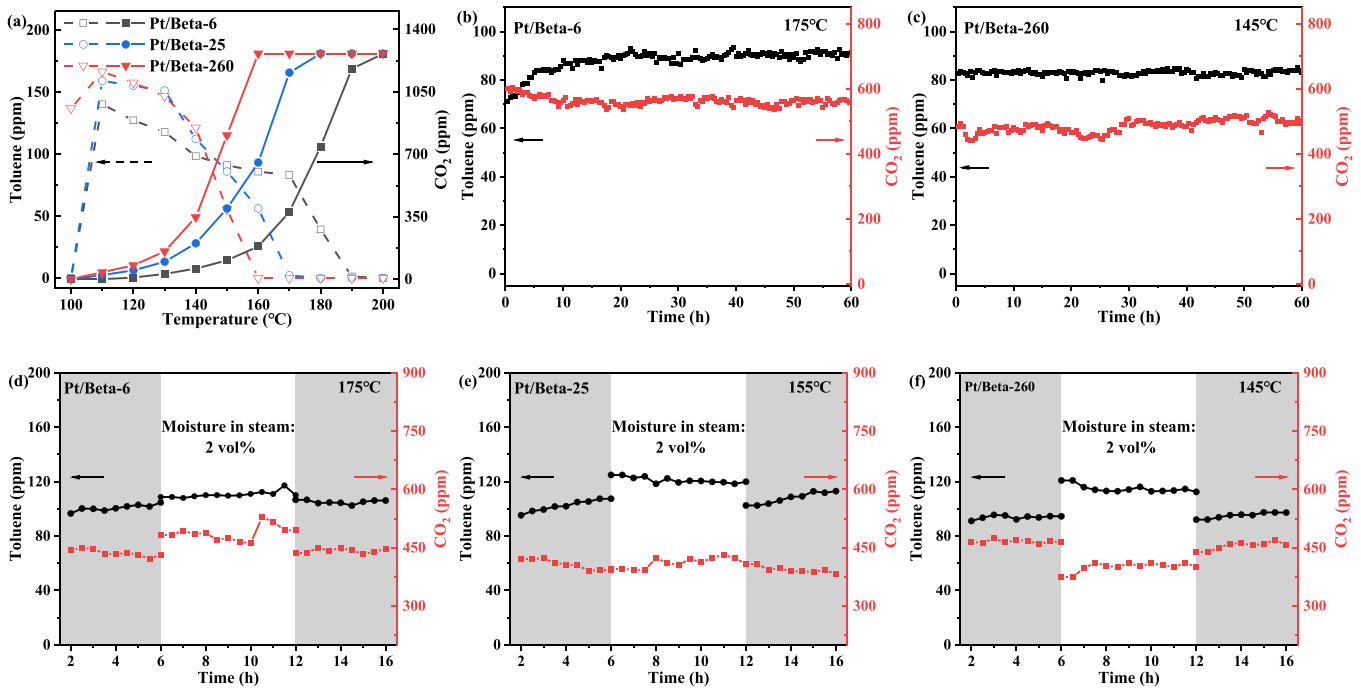

Fig. 1. (a) Toluene conversion and CO_2 generation as a function of temperature for different samples; the durability of (b) Pt/Beta-6 and (c) Pt/Beta-260; water vapor effect on toluene conversion and CO_2 generation for (d) Pt/Beta-6, (e) Pt/Beta-25 and (f) Pt/Beta-260 for 2 vol% water vapor.

might explain the lack of carbon deposition [20,21,33]. Considering the presence of water vapor in the atmospheric environment, the catalytic oxidation against toluene was also determined under 2 vol% water vapor at T_{50} of toluene conversion (Fig. 1(d), (e) and (f)). It was seen that the concentration of toluene increased for all samples when water vapor was introduced. Interestingly, the catalytic activity of toluene oxidation increased over Pt/Beta-6 and Pt/Beta-25. In particular, Pt/Beta-6 generated more CO_2 in the presence of water vapor, which was different from the high water resistance of high-silica zeolites reported in many literature studies [24,34]. When water vapor was turned off, all samples were able to return to their initial oxidation ability. The catalytic performance and water effects were significantly distinct on catalysts with different Si/Al ratios, probably attributed to the effect of acid sites on the characteristics of active sites such as the valence, location, and dispersion of Pt, etc., which were systematically explored in the following analysis via a series of designed characterization experiments.

3.2. Structural characterization

The BET surface area and micropore and mesopore information of Beta zeolites with different Si/Al ratios are shown in Table 1. All samples had excellent BET surface area, which was beneficial to the dispersion and anchoring of the noble metal. Comparing the Beta zeolite supports with the Pt/Beta catalysts, it could be found that the Pt loading led to slight decreases in the BET surface area, micropore surface area and volume, which might be caused by some Pt being distributed on the surface and some entering the channels of the Beta supports. At the same time, the average pore width showed a certain increase after Pt loading, which might be due to Pt occupying a portion of the micropores.

The XRD patterns of samples are shown in Fig. 2, all of which showed the characteristic diffraction peaks of BEA zeolites. Comparing the patterns of the Beta supports with those of the Pt/Beta catalysts, all samples had similar XRD patterns, meaning that the crystal structure of the Beta zeolites was unchanged after Pt loading. In particular, the characteristic diffraction peaks of Pt species at 39.76° (111) and 46.2° (200) were not observed in the pattern of Pt/Beta-6 [35,36], implying good dispersion of Pt. With the increase in Si/Al ratios, the characteristic

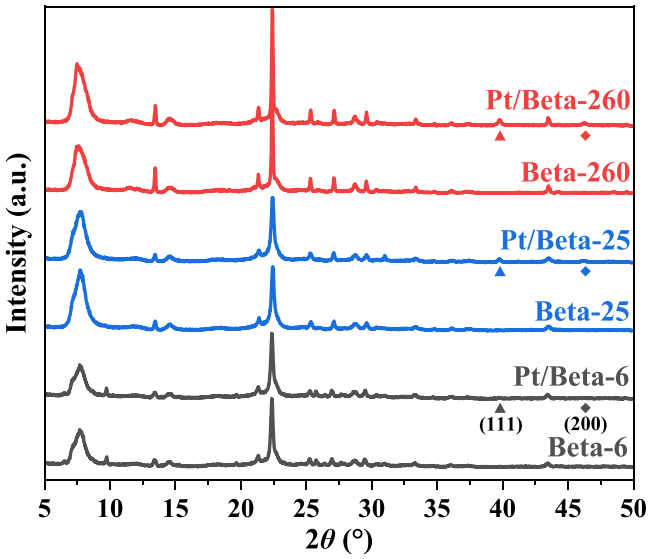

Fig. 2. XRD patterns of Beta and Pt/Beta with various Si/Al ratios.

diffraction peaks of Pt appeared, especially on the Pt/Beta-260 sample, indicating that the crystallinity of Pt in the samples increased with the increase in Si/Al ratios. This might be due to Pt accumulation in the Beta zeolites, resulting in the formation of Pt clusters and particles. FESEM images of the Pt/Beta-6, Pt/Beta-25 and Pt/Beta-260 catalysts are shown in Fig. S2(a, b, c), respectively. Only a few large particles of Pt could be seen in the FESEM images. The size of visible Pt particles was about 30–100 nm in Pt/Beta. In addition, the average particle size of Pt^0 in Pt/Beta-260 was about 30 nm estimated from the XRD spectra of Pt (111) at $2\theta = 39.7°$ according to Scherrer equation (Fig. 2), which was similar with the reported Pt size in Pt/ZSM-5 catalyst [37]. The results of EDX elemental mappings exhibited that the Pt particle distribution was consistent with those of Si and Al, illustrating that Pt was well-dispersed in all Pt/Beta catalysts, especially Pt/Beta-6 (Fig. S2(a1-a3, b1-b3,

c1-c3)), which was also confirmed by the XRD results.

3.3. Surface chemical state of Pt

XAFS experiments were carried out to determine the valence state of the loaded Pt and the coordination environment of Pt species. The normalized Pt L_3 edge X-ray absorption near edge structure (XANES) spectra of Pt/Beta-6, Pt-Beta-25, Pt/Beta-260 and reference Pt foil and PtO_2 standard samples are shown in Fig. 3(a). The normalized results manifested the differences in the Pt valence in the samples. The white-line (Pt L_3 edge) intensity of Pt/Beta with various Si/Al ratios was between those of the Pt foil and PtO_2 standard samples, indicating that the valence state of Pt in all samples was between Pt^0 and Pt^{4+}. With the increase in Si/Al ratios, the white-line intensity and position shifted towards those of Pt foil. This phenomenon suggested that Pt was present in the metallic state in the high-silica Pt/Beta catalysts. In order to obtain the coordination environment of Pt species, the K_3-weighted Fourier transform Extended X-ray absorption fine structure (EXAFS) spectra were measured as shown in Fig. 3(b). The EXAFS results showed only one significant peak at 1.65 Å on Pt/Beta-6. With further increase in the Si/Al ratio, this peak decreased in intensity as another peak appeared at 2.61 Å; this second peak became the most prominent peak on Pt/Beta-260. The peak at 1.65 Å was attributed to the Pt-O and the peak at 2.61 Å represents Pt-Pt [38,39]. Therefore, it was speculated that Pt was highly dispersed on Pt/Beta-6 in the form of $Pt^{\delta+}$. With the increase in the Si/Al ratios, the dispersion of Pt on Pt/Beta-25 and Pt/Beta-260 decreased, mainly existing as low-valence Pt NPs. For Pt/Beta-260, virtually all Pt appeared to be contained in Pt^0 NPs.

In order to further confirm the chemical states of Pt, *in situ* DRIFTS of adsorbed CO over various Pt/Beta catalysts at room temperature were measured and presented in Fig. 3(c). The IR spectral peaks above 2100 cm^{-1} corresponded to the adsorption of CO on $Pt^{\delta+}$, and the band below 2100 cm^{-1} was assigned to linearly bonded CO on Pt^0 NPs [40, 41]. To identify the state of Pt species, FTIR spectroscopy of CO adsorption had performed by Hadjiivanov and co-workers over Pt-H-ZSM-5, characteristic peaks located at 2165 and 2150 cm^{-1} for $Pt^{2+}(CO)_2$, below 2100 cm^{-1} for Pt^0-CO [41]. In our case, the peaks at 2171, 2150, and 2133 cm^{-1} appeared on Pt/Beta-6 and Pt/Beta-25. Thus, the existence of Pt^{2+} was confirmed on Pt/Beta-6 and Pt/Beta-25, which might include $Z[Pt^{2+}(OH)]^+$ ions balanced by a single Al site, where Z represents an ion-exchange site, and Pt^{2+} associated with paired Al sites (Z_2Pt^{2+}), etc (with detailed information in Fig. S3). Combining the results of XRD, FESEM, XAFS, and *in situ* FTIR spectra of CO adsorption, it was concluded that Pt mainly existed in the form of well-dispersed oxidized Pt ($Z[Pt^{2+}(OH)]^+$, Z_2Pt^{2+} and other $Pt^{\delta+}$ species) when the Si/Al ratio was low. With the increase in the Si/Al ratio, Pt in Pt/Beta-25 existed in the form of $Pt^{\delta+}$ and Pt^0. Furthermore, particle clusters of metallic Pt were the main form of Pt on Pt/Beta-260. In addition, adsorbed CO was completely desorbed from the surface after Pt/Beta-260 was purged with N_2 at 30 °C (Fig. S4), indicating that the adsorption of CO on Pt/Beta-260 was weak.

The H_2-TPR experiment was used to investigate the redox properties

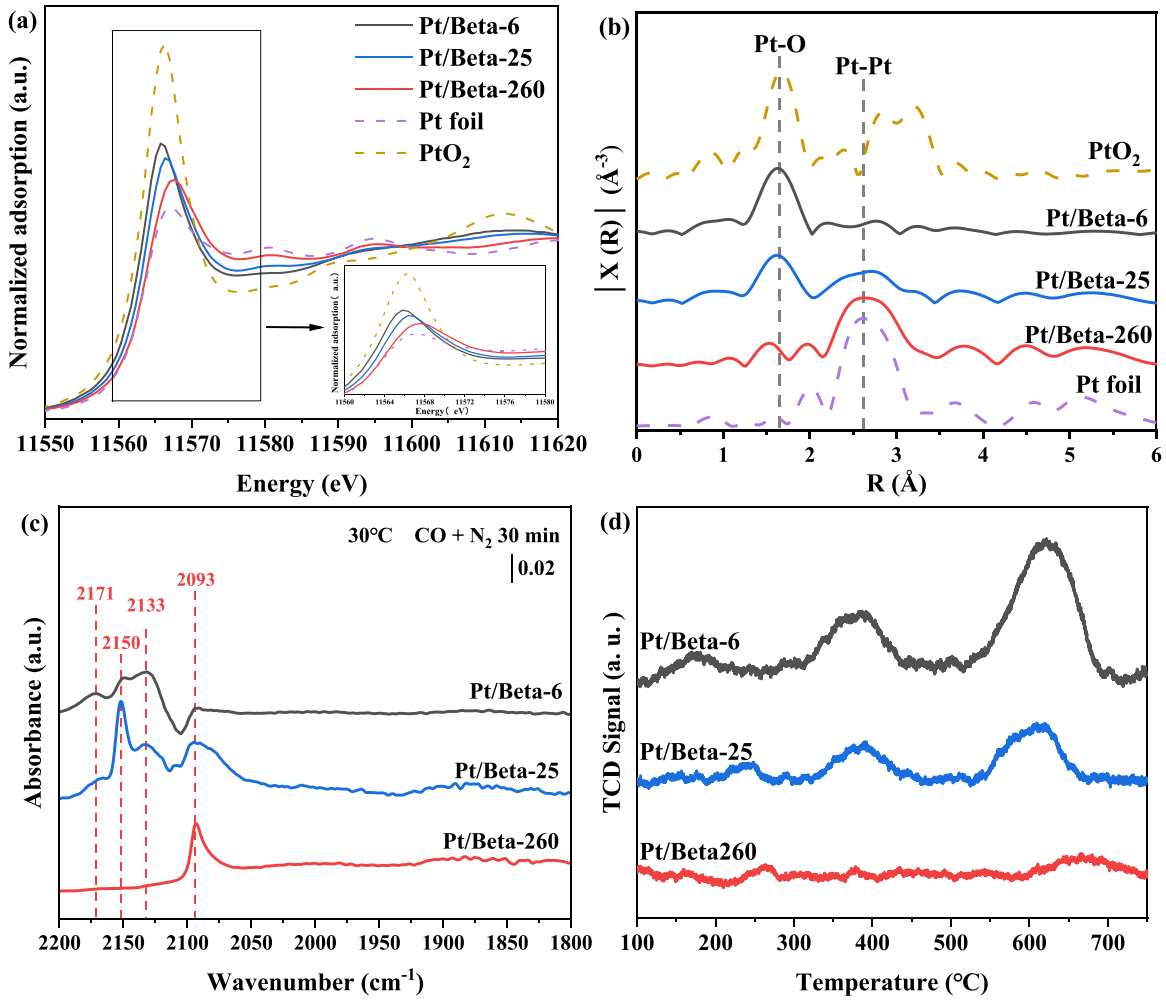

Fig. 3. (a) Pt L_3 edge XANES spectra and (b) K_3-weighted Fourier transform EXAFS spectra of Pt/Beta-6, Pt-Beta-25, Pt/Beta-260 and the reference standard samples (Pt foil and PtO_2); (c) *in situ* FTIR spectra of adsorbed CO over different catalysts at 30 °C; (d) H_2-TPR profiles of all catalysts.

of the catalysts. The H_2-TPR results for all the Beta supports with no Pt loading exhibited that there was no consumption of H_2 (Fig. S5(a, b, c)). However, after Pt loading, various reduction peaks with different intensities appeared (Fig. 3(d)). For Pt/Beta-6, three reduction peaks occurred at different temperatures. The reduction peak at around 200 °C was attributed to the reduction of $Pt^{\delta+}$ ions on the zeolite surface and/or in the main channels of the Beta zeolite. Another major peak around 380 °C probably related to the reduction of $Pt^{\delta+}$ at the ion exchange site and reduction peaks around 600 °C might be attributed to the reduction of Pt on silanol which had a strong interaction with Beta zeolite [42,43]. For Pt/Beta-25, the reduction peaks were similar to those on Pt/Beta-6, but the intensity of the peaks was significantly decreased. For Pt/Beta-260, almost no reduction peaks appeared due to the existence of Pt^0.

For comparison, the activities of Pt/Beta-N zeolite catalysts prepared from the different Pt source of $Pt(NO_3)_2$ were also examined (Fig. S6(a)). The results showed that Pt/Beta-260 could completely oxidize toluene at around 160 °C, while when Pt/Beta-260-N was used, the toluene conversion efficiency was only about 20% at 160 °C. As indicated by XRD patterns (Fig. S6(b)), no characteristic diffraction peaks of Pt observed on Pt/Beta-260-N, indicating better dispersion of Pt than that on Pt/Beta-260. Such high dispersion of Pt on Pt/Beta-260-N was further revealed by FESEM images and EDX elemental mappings (Fig. S6(c)). H_2-TPR curves of Pt/Beta-260 and Pt/Beta-260-N were compared and a reduction peak appeared at around 600 °C for Pt/Beta-260-N (Fig. S7 (a)), which might be due to the reduction of $Pt^{\delta+}$ on silanol. On Pt/Beta-260-N, *in situ* DRIFTS of CO adsorption (Fig. S7(b)) also suggested that Pt mainly existed in the form of $Pt^{\delta+}$. What's more, XANES (Fig. S7(c)) and EXAFS (Fig. S7(d)) showed that the white line of Pt/Beta-260-N was more inclined to Pt^{4+}, which was quite different from that on Pt/Beta-260. Therefore, different Pt source led to significant distinct in the valence and dispersion of Pt, finally relating to quite different redox properties and catalytic performance. Thus, it could be deduced that the $Pt(NH_3)_4(NO_3)_2$ using for the preparation of Pt/Beta-260 could benefit the formation of Pt^0 particles [44]. These results also proved that Pt^0 particles had excellent catalytic oxidation ability towards toluene.

The NH_3-TPD curves used to measure acid sites are shown in Fig. 4 (a), (b) and (c), which could be fitted by two distinct peaks. The peak at low temperature (200–300 °C) represents the adsorption of NH_3 on weak acid sites, and the high temperature (350–400 °C) peak is due to strong Brønsted acid sites [14,19,45,46]. The acid sites of Beta zeolites decreased significantly with increase in the Si/Al ratios. The distributions of acid sites on the Beta supports and Pt/Beta catalysts were determined. It was demonstrated that the numbers of strong Brønsted acid sites were significantly increased for the Pt/Beta-6 and Pt/Beta-25 samples. Since Beta-260 had few acid sites, the introduction of Pt had little effect on acid sites. The bridging hydroxyls (Si(OH)Al) are often considered as the relevant coordination bonds causing the catalysts to have strong Brønsted acidity [47,48]. The increase in Brønsted acid sites on the Pt/Beta catalysts also proved that Pt was loaded on the bridge hydroxyl sites (Si(OH)Al). Especially, $Z[Pt^{2+}(OH)]^+$ might be helpful for the increase of Brønsted acid sites [49].

The ^{27}Al MAS NMR and ^{29}Si MAS NMR spectra of all samples are shown in Fig. 4(d) and (e). The ^{27}Al MAS NMR spectra had a noticeable peak at 55 ppm, corresponding to the four-coordinate framework Al (FAl (IV)) which directly determined the position of the bridging

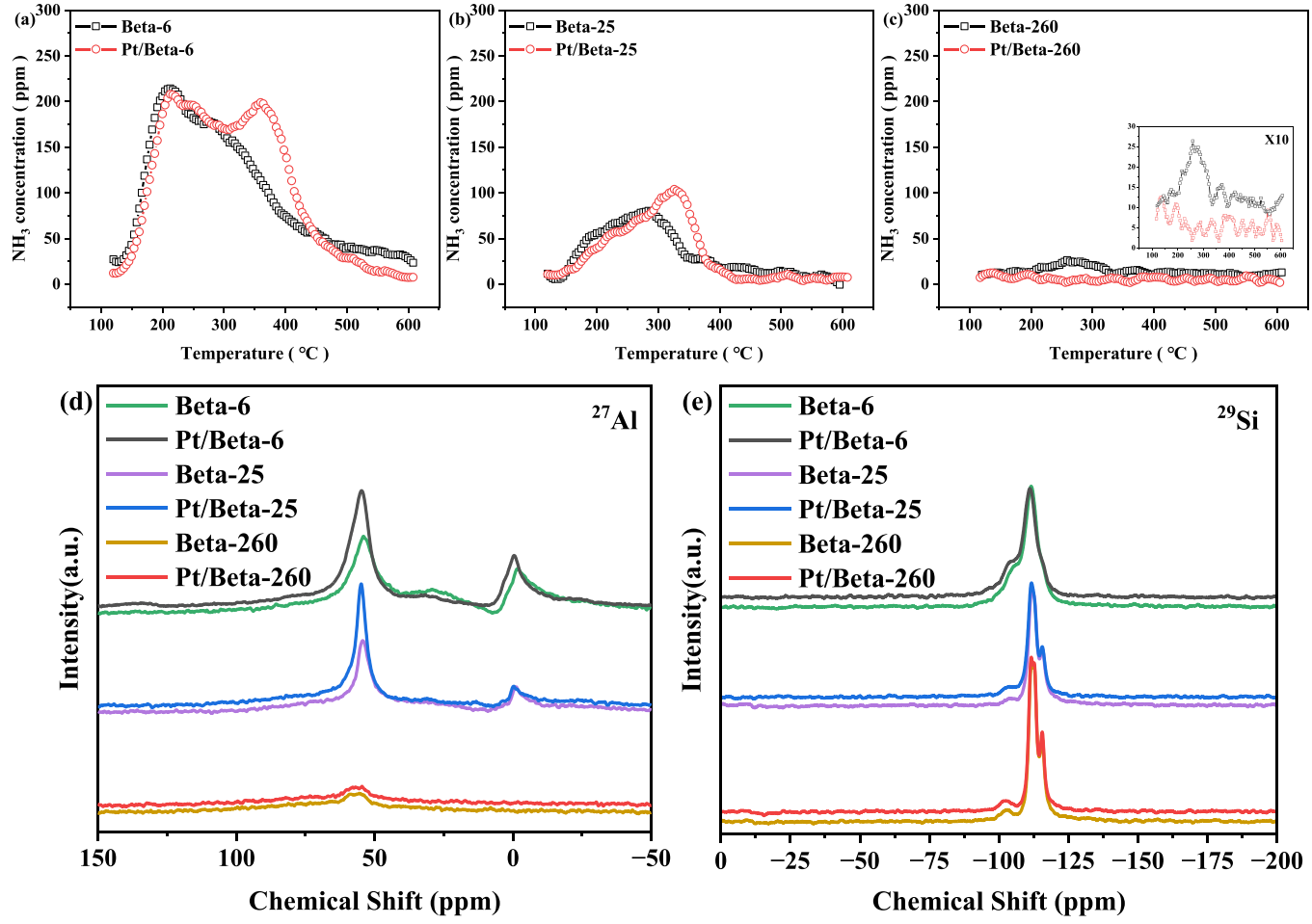

Fig. 4. NH_3-TPD of Beta supports and Pt/Beta catalysts ((a) Beta-6 and Pt/Beta-6, (b) Beta-25 and Pt/Beta-25; (c) Beta-260 and Pt/Beta-260; (d) ^{27}Al MAS NMR and (e) ^{29}Si MAS NMR spectra of all samples.

hydroxyl groups [50,51]. Comparing the Beta supports and Pt/Beta catalysts, the ^{27}Al MAS NMR signals showed that the position of chemical shift of FAl changed slightly after Pt loading, which indicated that its coordination environment had changed [52], and also proved that Pt^{2+} were mainly located on the bridge hydroxyl groups [51], which was consistent with the results of NH_3-TPD [53]. Moreover, the peak at 0 ppm was attributed to the octahedrally coordinated extra-framework aluminum species (EFAL), which may serve as electron acceptors and Lewis acid sites [51]. Also, it was reported that EFAL were plausible sites for Pt anchoring onto the surface of the Beta zeolites [53]. However, in the case of Beta-6, there was only slight change of NH_3-TPD peaks at around 200 °C related to EFAL before and after Pt loading (Fig. 4) [49].

Additionally, FTIR spectra of Beta and Pt/Beta were measured. In this case, the bands at 3742, 3733, and 3700 cm^{-1} could be assigned to Si-OH groups of Pt/Beta (Fig. 5). In more detail, the bands at 3742 and 3733 cm^{-1} could be attributed to terminal silanol groups and internal silanol groups, respectively [54]. The bands at 3775,3661, and 3602 cm^{-1} were related to isolated Al-OH of Beta zeolites, Al-OH groups (EFAL), bridging Si(OH)Al groups (Brønsted acid sites), respectively [54]. After Pt loading, a marked decrease in the Brønsted acid peak (3602 cm^{-1}) observed in the case of Si/Al = 6, while no obvious change of EFAL (3661 cm^{-1}) was observed. This result also indicated the consumption of Brønsted acid sites with the introduction of Pt. Therefore, it could be deduced that EFAL did not play important role on anchoring Pt. After Pt introduced, meanwhile, it was noting that an intense band appeared at 3729 cm^{-1}, which could be associated with the O-H stretch from $Z[Pt^{2+}(OH)]^+$ (Fig. S3) [49]. Such assignment can be drawn from the results of EXAFS, *in situ* DRIFTS of adsorbed CO, H_2-TPR, NH_3-TPD, NMR, and FTIR spectra. When Si/Al increased to 260, a marked broad band of H-bond Si-OH groups at 3510 cm^{-1} arose, revealing the presence of vacant T-sites associated with silanol groups [54]. After Pt loading on Beta-260, the intensity of peaks at 3733, 3700, and 3510 cm^{-1} decreased, suggesting that silanol groups as well as correlative vacant were consumed.

In order to clarify the changes of Pt, we have characterized the used samples by FESEM together with EDX elemental mappings, XRD, XANES and EXAFS, and *in situ* DRIFTS of adsorbed CO, and compared with those of fresh samples. Based on the results of FESEM, EDX, and XRD (Fig. S2 and Fig. S8), it could be seen that the particle size of Pt was hardly changed after reaction. XANES spectra showed that the white line (Pt L_3 edge) intensity and position of used Pt/Beta (denoted as Pt/Beta-U thereafter) shifted towards those of Pt foil, and this change trend became weaker with the increase of Si/Al ratios (Fig. S9). EXAFS spectra exhibited that the intensity of Pt-O bonds on Pt/Beta-6-U and Pt/Beta-25-U decreased, while the intensity of Pt-Pt bonds increased, indicating that part of $Pt^{\delta+}$ might be reduced in the process of toluene catalytic oxidation (Fig. S10). EXAFS spectra also showed that both Pt/Beta-260 and Pt/Beta-260-U mainly existed in the form of Pt^0 NPs and the valence of Pt had little change after reaction. *In situ* DRIFTS measurements (Fig. S11) showed that the intensity of peak around 2083–2093 cm^{-1} assignable to adsorbed CO on Pt^0 increased after reaction [41], which confirmed the reduction of $Pt^{\delta+}$ into Pt^0. During the catalytic oxidation of toluene, some species with reducibility such as CO were produced, possibly leading to the reduction of $Pt^{\delta+}$ [41]. It could be deduced that the reduction of $Pt^{\delta+}$ into Pt^0 during the reaction process might be beneficial to the sharp decrease of toluene and quick increase of oxidation ability for low-silica Pt/Beta at above 170 °C (Fig. 1(a)). As for Pt/Beta-260-U, the intensity of peak related to adsorbed CO on Pt^0 decreased, indicating weaker adsorption of CO on used sample (Fig. S4 and Fig. S11).

3.4. Mechanism of catalytic oxidation reaction

In order to clarify the desorption performance and roles of active oxygen species, Toluene-TPD-MS experiments were carried out with temperature programmed desorption in a He atmosphere. Fig. 6(a-f) shows that besides toluene ($m/z = 92$) and CO_2 ($m/z = 44$) desorbed from the Pt/Beta, benzaldehyde ($m/z = 106$), benzene ($m/z = 78$), CO ($m/z = 28$) and H_2 ($m/z = 2$) formation also occurred [55]. Only one desorption peak of toluene appeared on all samples, and Pt loading on the Beta supports had no effect on the desorption temperature. The toluene desorption temperature increased due to the more abundant acid sites on the low-silica Beta zeolites resulting from the stronger chemisorption of toluene. This could also explain why toluene was more easily adsorbed on low-silica Pt/Beta catalysts in the activity test (Fig. 1 (a)). Moreover, formation of benzaldehyde and benzene (Fig. 6(b) and (c)) was observed on low-silica Beta zeolite supports, and as the Si/Al ratio increased, the intensity of desorption peaks and desorption temperatures of benzaldehyde and benzene gradually decreased. Almost no benzaldehyde or benzene were observed on Beta-260 zeolites. Moreover, it was proposed that the EFAL species may serve as Lewis sites, contributing to both a substantially higher *para* selectivity in toluene disproportionation and its alkylation with ethylene, and to an increased rate of side reactions leading to the zeolite deactivation by coke formation in toluene alkylation with ethylene [56]. In our case, Lewis sites associated with EFAL might influence the adsorption and catalytic performances, considering that strong chemisorption of toluene occurred on low-silica Beta zeolite supports, which was followed by the formation of benzaldehyde and benzene. When Pt was loaded, there was also no benzaldehyde formation, while more benzene formed in the gas phase. This indicated the formation of more surface and/or lattice oxygen species after loading of Pt on the Beta zeolites, leading to enhanced oxidation of toluene. Furthermore, CO, H_2 and CO_2 were also generated in Toluene-TPD-MS (Fig. 6(d-f)). On Pt/Beta-6, the introduction of Pt resulted in a large amount of CO and H_2 generation at 280 °C and 462 °C. It could be deduced that the loading of Pt promoted the formation and activation of hydroxyl groups, followed by the main reaction

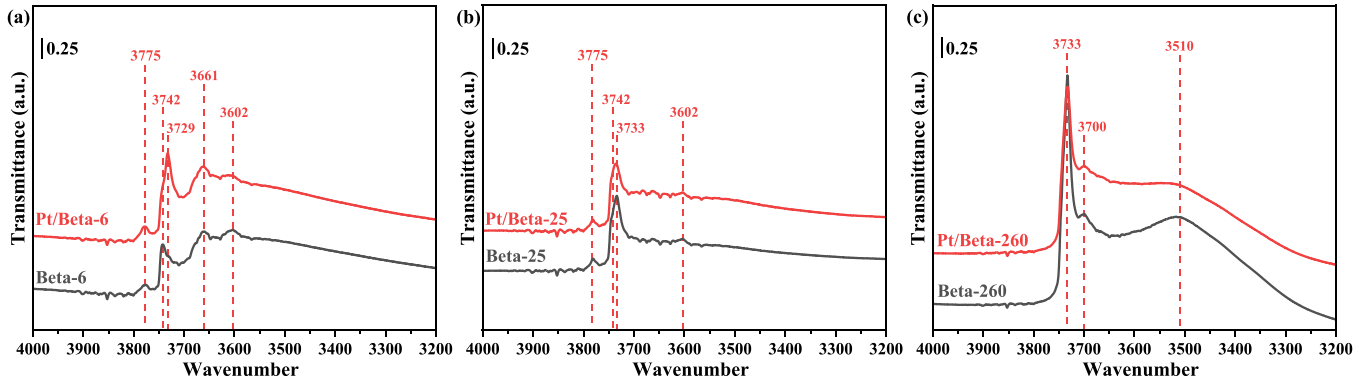

Fig. 5. Transmission IR spectra of (a) Beta-6 and Pt/Beta-6, (b) Beta-25 and Pt/Beta-25, (c) Beta-260 and Pt/Beta-260 under vacuum.

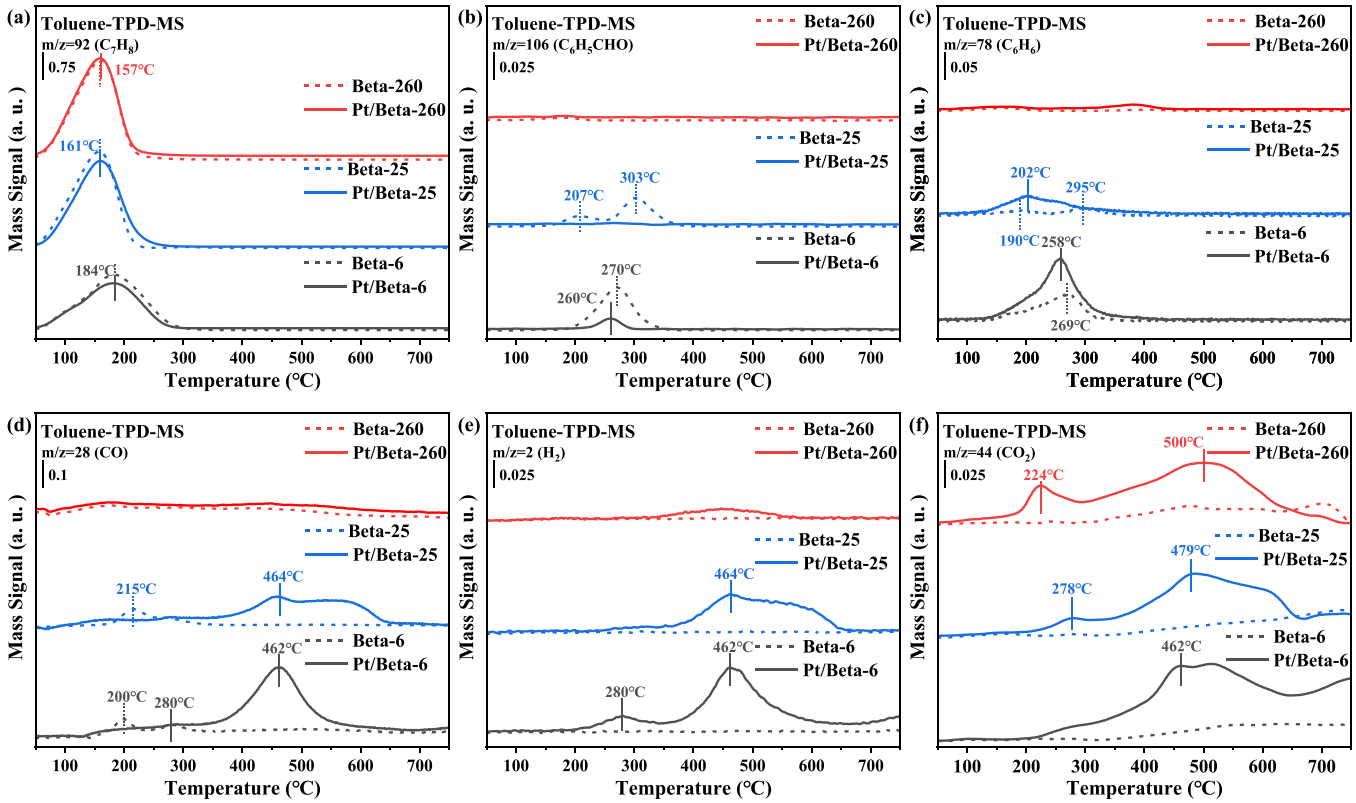

Fig. 6. Toluene-TPD-MS for Beta supports and Pt/Beta catalysts; Desorption peaks of (a) C_7H_8, (b) C_6H_5CHO, (c) C_6H_6, (d) CO, (e) H_2, (f) CO_2.

2 C+ 2OH→2CO+H_2, since CO and H_2 were generated at the same temperatures. It was further verified that the Pt^{2+} ions were adsorbed on the ion-exchange sites of the bridged hydroxyls (Si(OH)Al), which then introduced additional hydroxyl groups as $Z[Pt^{2+}(OH)]^+$. Toluene-TPD-MS results (Fig. 6(d) and (f)) also proved that there were some OH groups closely related to $Pt^{\delta+}$ since the formation amounts of CO and H_2 increased with the increase of ion-exchange sites of Pt/Beta and almost no H_2 formation on all pure Beta supports. At the same time, the oxidation of CO was also further enhanced, reacting with the hydroxyl groups of $Z[Pt^{2+}(OH)]^+$ and other active oxygen species to generate CO_2 through the reactions 2CO+ 2OH→2CO_2 +H_2 and CO+O→CO_2 [57,58]. The promotion effect of H_2O on the oxidation of toluene into CO_2 on low-silica Pt/Beta (Fig. 1(d) and (e)) could be explained based on these analyses. $Pt^{\delta+}$ ions could transform H_2O and O_2 into active hydroxyl groups according to the reaction O_2 +H_2O→O* +2OH. The produced OH groups played important role for oxidizing toluene to CO_2 on low-silica Pt/Beta, which was confirmed by the results of Fig. 6. In the case of high-silica Pt/Beta, Pt species were mainly presented as Pt^0. In the presence of H_2O, theoretical study revealed that the Pt^0 was not easy to active O_2 because the physiosorbed state of O_2 is only favorable when densely packed Pt (111) surface was covered with adsorbed OH/H_2O [59]. As a result, water vapor decreased toluene conversion and the concentration of CO_2 over Pt/Beta-260 (Fig. 1(f)).

The reaction pathways for CO, H_2, and CO_2 formation on Pt/Beta-25 were similar to those on Pt/Beta-6, but smaller amounts of these species were produced due to the presence of fewer hydroxyl groups. However, for Pt/Beta-260, a significant difference with Pt/Beta with low silica was observed. Only small amounts of benzaldehyde, benzene, CO, and H_2 were formed. It was worth noting that the amount of CO_2 produced was high and the temperature of CO_2 appearance was the lowest among the catalysts, demonstrating that surface adsorbed oxygen and lattice oxygen species except hydroxyl groups enhanced the oxidation of toluene in the case of high-silica Pt/Beta with Pt^0 active sites.

To specifically explore the distinct mechanism of the activation and supply of oxygen over Pt/Beta catalysts and the roles of reactive oxygen species in the catalytic oxidation of toluene, Toluene-TPSR-MS experiments were performed in an $^{18}O_2$ reaction atmosphere. The catalysts first adsorbed toluene to reach saturation, and then different Pt/Beta catalysts were heated to 750 °C with the introduction of $^{18}O_2$, and the results are shown in Fig. 7(a-c). The temperatures of toluene desorption and benzene formation were consistent with the results of Toluene-TPD-MS. Pt/Beta-260 could oxidize toluene to CO_2 and CO at the lowest temperature, 217 °C, exhibiting the best ability to activate and supply oxygen. Besides toluene, benzene, CO and CO_2, no other species, such as benzaldehyde or H_2, appeared in the Toluene-TPD-MS spectra, indicating that these intermediates could be further oxidized or not formed in the presence of oxygen. Interestingly, there were significant differences between Pt/Beta with high silica and low silica regarding the activation of O_2 and supplementation of reactive oxygen species. CO and CO_2 were mainly generated in the form of $C^{16}O$, $C^{16}O_2$ and $C^{18}O^{16}O$ over Pt/Beta-6, while over Pt/Beta-260, reactive oxygen species were almost entirely derived from $^{18}O_2$. It could be deduced that the oxidation reaction of toluene on Pt/Beta-6 was mainly due to the hydroxyl groups of $Z[Pt^{2+}(OH)]^+$ and other active oxygen species which were generated on Pt/Beta-6, and $^{18}O_2$ supplemented the reactive oxygen species of the catalysts and/or directly was activated to participate reaction. However, on Pt/Beta-260, which directly activated $^{18}O_2$, the oxidation reaction of toluene easily took place. Thus, Pt^0 NPs on the Pt/Beta-260 were responsible for its better ability to activate O_2 and oxidize toluene with the beneficial supplementation of reactive oxygen species.

In order to explore the intermediate products and reaction mechanism towards toluene and oxygen over Pt/Beta catalysts, *in situ* DRIFTS of toluene adsorption and oxidation processes over Pt/Beta-6, Pt/Beta-25 and Pt/Beta-260 are shown in Fig. 8(a), (b) and (c). After the adsorption of toluene on Pt/Beta-6 in N_2 atmosphere for 30 min, absorption peaks appeared at 3028 cm^{-1} representing the C-H stretching vibration of benzene rings, and the peaks observed at 2924 and

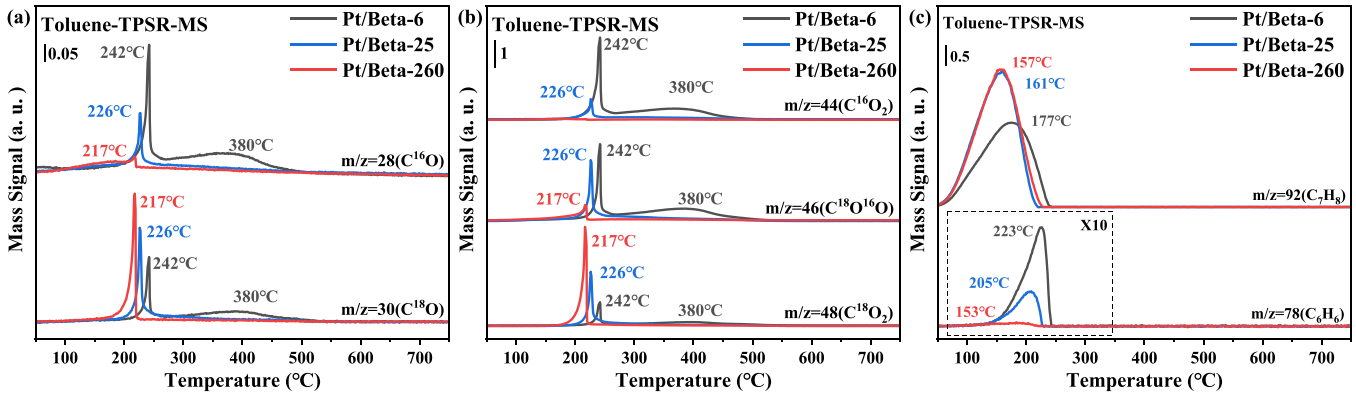

Fig. 7. Toluene-TPSR-MS for different catalysts under $^{18}O_2$: (a) CO, (b) CO_2, (c) benzene and toluene.

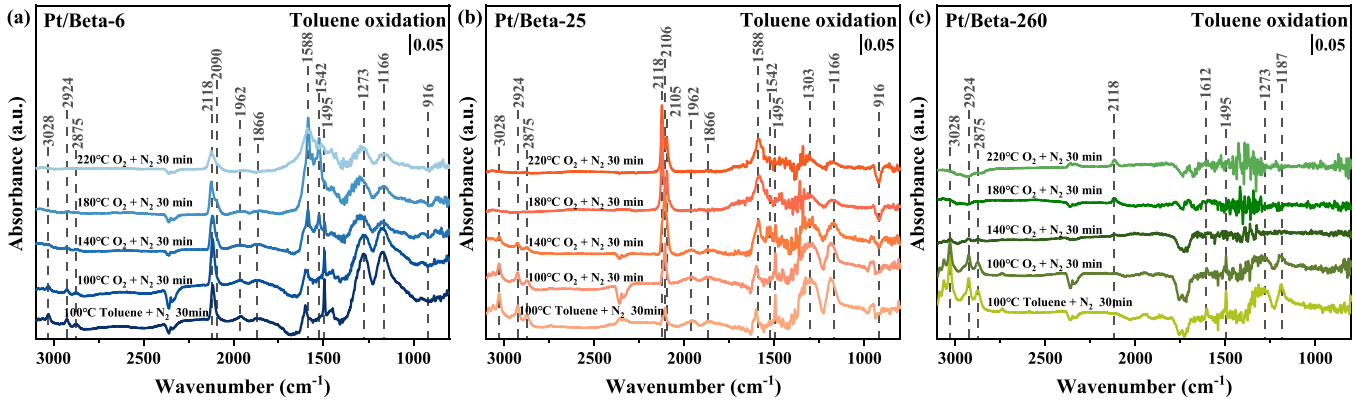

Fig. 8. *In situ* DRIFTS of toluene adsorption and oxidation process over (a) Pt/Beta-6, (b) Pt/Beta-25 and (c) Pt/Beta-260.

2875 cm^{-1} were assigned to the C-H stretching vibration on methyl groups [60]. The peaks at 1495 cm^{-1} represented the stretching vibration of the C=C double bond in the benzene rings [61]. This indicated that toluene was adsorbed on the Pt/Beta-6 surface. What's more, the characteristic peaks between 1320 and 1270 cm^{-1} were attributed to the -CH_2 deformation vibration, and those from 1200 to 1160 cm^{-1} were assigned to the C-O stretching vibration of benzylic species [62]. The characteristic absorption peaks at 2120–2100 cm^{-1} were attributed to CO, and the peaks at 2000–1800 cm^{-1} were assigned to the C=C double bond stretching vibration; combined with the 915 cm^{-1} band, this indicated that a five-membered cyclic anhydride and maleic acid were produced [63]. It was verified that toluene chemically adsorbed on Pt/Beta-6 and was then oxidized into intermediate products such as benzyl alcohol, five-membered cyclic acid anhydride and maleic acid, and CO, indicating that toluene could partially be oxidized as a result of its own hydroxyl groups and/or other reactive oxygen species in a N_2 atmosphere. With the introduction of oxygen, the peaks represented by toluene and benzyl alcohol gradually weakened, while the peaks at 1588 and 1542 cm^{-1} became more and more prominent, which were assigned to the stretching vibration of the C=C bonds on the backbone and the asymmetric stretching vibration of -COO bonds of carboxylate species, respectively [64,65]. This demonstrated that the toluene and benzyl alcohol adsorbed on the Pt/Beta-6 would be further oxidized to benzoic acid in the presence of sufficient oxygen and that five-membered cyclic anhydrides and maleic acid were generated at the same time. From the results of toluene adsorption and oxidation at different temperatures (Fig. 8, S12-S14), it was found that the rate of catalytic oxidation increases with the increase in temperature. The reaction products and pathway of toluene on Pt/Beta-25 were almost identical to those on Pt/Beta-6. However, on Pt/Beta-260, only a small amount of benzyl alcohol and CO were detected on the surface of catalysts. This might be due to the fact that the catalysts had strong oxidation ability and high reaction rate. In addition, the catalysts did not easily adsorb CO (Fig. S4) and CO was oxidized directly in gas phase when O_2 was introduced.

Fig. S15 showed the gas-phase product analysis results during the warming process of the catalytic combustion of toluene. For Pt/Beta-6, a small amount of benzene and acetic acid were detected at 120 °C. On increasing the temperature to 190 °C, more benzene was generated. However, almost no benzene was generated in the whole process for Pt/Beta-260, which was consistent with the Toluene-TPSR-MS results (Fig. 7). What's more, benzoic acid was formed at the low temperature of 60 °C for Pt/Beta-260, indicating that high-silica Pt/Beta catalysts had superior low-temperature activity and reaction rate in the catalytic oxidation reaction of toluene.

In order to elucidate the adsorption configurations of toluene and oxygen of Pt/Beta catalysts, DFT simulation was carried out [29]. Pt_{13}/BEA and Pt/BEA-Al were simulated to investigate Pt/Beta-260 (Pt^0) and Pt/Beta-6 ($Pt^{\delta+}$), respectively. A comparison of the adsorption energies of both catalysts for toluene and oxygen are shown in Fig. 9. It was clear that Pt_{13} (Pt^0) nanoparticles had a stronger ability to adsorb toluene and oxygen than isolated $Pt^{\delta+}$ sites. The differences in O_2 and toluene electron densities at different Pt positions on Pt/BEA catalysts are also shown in Fig. 10. A positive difference in the charge layer (yellow in the Fig. 10), indicates that the electron density increased after adsorption and a negative value means a decrease in charge density (blue in the Fig. 10). Comparing Pt_{13}/BEA with Pt/BEA-Al, Pt_{13} transferred more electrons to O_2 and toluene, while the change in the O_2 and toluene charge density on $Pt^{\delta+}$ adsorption was very weak, illustrating that Pt^0 nanoparticles had stronger activation ability for oxygen and toluene. This also explained why the Pt/Beta-260 catalyst could more efficiently activate gaseous oxygen for further oxidizing toluene. The activation of O_2 over both catalysts were also verified by searching of

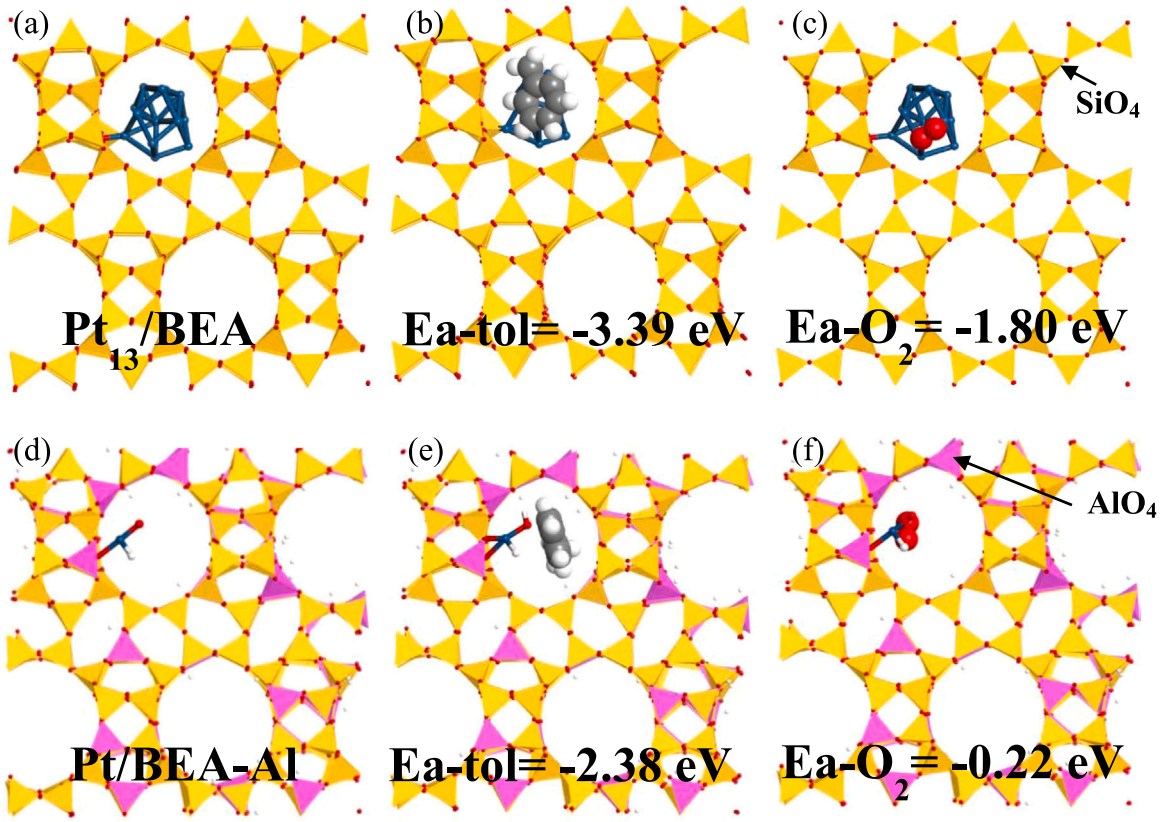

Fig. 9. Adsorption configuration and energy of toluene and O_2 in the Pt_{13}/BEA catalyst ((a), (b) and (c)) and Pt/BEA-Al catalysts ((d), (e) and (f)). (Red: O, navy blue: Pt, white: H, gray: C, yellow: SiO_4 tetrahedral, pink: AlO_4 tetrahedral).

transition state. As illustrated in Fig. S16, the activation barrier over the local interface of Pt_{13}/BEA (Pt^0) was 0.31 eV, which was much lower than that of Pt/BEA-Al ($Pt^{\delta+}$). Therefore, the presence of Pt^0 particles was beneficial to activate of O_2. Pt/Beta-260 with Pt^0 NPs was more active than the Pt/Beta-6 with $Pt^{\delta+}$ in toluene oxidation, which was consistent with adsorption results as shown in Figs. 9 and 10.

Based on the experimental results and corresponding analysis, the reaction pathway of toluene on Pt/Beta catalysts could be deduced. In the case of low-silica Pt/Beta, both hydroxyl groups ($Z[Pt^{2+}(OH)]^+$) and other active oxygen species were responsible for toluene oxidation (Fig. 6). Toluene was first chemically adsorbed on the Pt/Beta catalysts in the form of benzyl alcohol. Benzyl alcohol was further oxidized to benzaldehyde and benzoic acid, which was prompted by the action of hydroxyl groups and other active oxygen species. Subsequently, the benzene ring was opened to generate CO_2 and H_2O with a small number of by-products, such as benzene, generated at the same time (Fig. 8). In the case of high-silica Pt/Beta, active oxygen species were produced and supplemented via efficiently activating O_2 by Pt^0 (Fig. 7 and Fig. S16). In the presence of active oxygen species, toluene could be rapidly oxidized to benzyl alcohol and then benzoic acid, and subsequently the benzene ring broke. During this process, there was little accompanying CO detected on the surface of high-silica Pt/Beta. This might be because that the catalysts did not easily adsorb CO (Fig. S4) and CO was oxidized directly in the gas phase in the presence of O_2. Compared with $Pt^{\delta+}$ of low-silica Pt/Beta, Pt^0 of high silica Pt/Beta was more favorable for the benzene ring opening reaction.

On low-silica Pt/Beta, it was worth mentioning that the reduction of $Pt^{\delta+}$ into Pt^0 occurred during the initial stage of toluene oxidation. Subsequently, Pt^0 probably played important role in the reaction of toluene, following similar reaction pathway occurred over high-silica Pt/Beta.

4. Conclusion

The regulatory effects of strong Brønsted acid sites on Pt/Beta catalysts with different Si/Al ratios on Pt active sites were studied, including valence states, location, dispersity, and ability to activate oxygen and oxidize toluene. The results showed that $Pt^{\delta+}$ in the low-silica Pt/Beta were the main active sites for toluene oxidation, one of which were $Z[Pt^{2+}(OH)]^+$ mainly located at the ion-exchange sites (strong Brønsted acid sites), resulting in superior water resistance on the basis of the role of hydroxyls. By contrast, Pt^0 NPs were the main active sites of high-silica Pt/Beta and gave enhanced catalytic performance due to excellent activation ability towards O_2 as well as effective supplementation of reactive oxygen species. Regardless of their acidity, all Pt/Beta catalysts had excellent stability and durability, achieved through increasing the dispersion of active sites based on isolated $Z[Pt^{2+}(OH)]^+$, together with the excellent coke deposition resistance of high-silica Beta. The strong ability of Pt^0 to activate O_2 and the reduction of $Pt^{\delta+}$ into Pt^0 during the reaction process might be contributed to improving catalytic activity and durability. Moreover, the Pt/Beta samples with different active sites exhibited somewhat distinct catalytic mechanisms in the process of toluene oxidation. Besides the formation of intermediates such as benzyl alcohol and benzoic acid, benzaldehyde and benzene also appeared in the case of low-silica Pt/Beta, while these intermediates hardly formed in the case of high-silica Pt/Beta, resulting from the promotion of the benzene ring opening reaction and oxidation ability by Pt^0.

CRediT authorship contribution statement

Daiqiang Li: Investigation, Data acquisition, Data curation, Data analysis, Writing – original draft. **Lian Wang:** Data curation, Data analysis, Writing – review & editing, Funding acquisition, Project administration. **Yuqing Lu:** Data acquisition. **Hua Deng:**

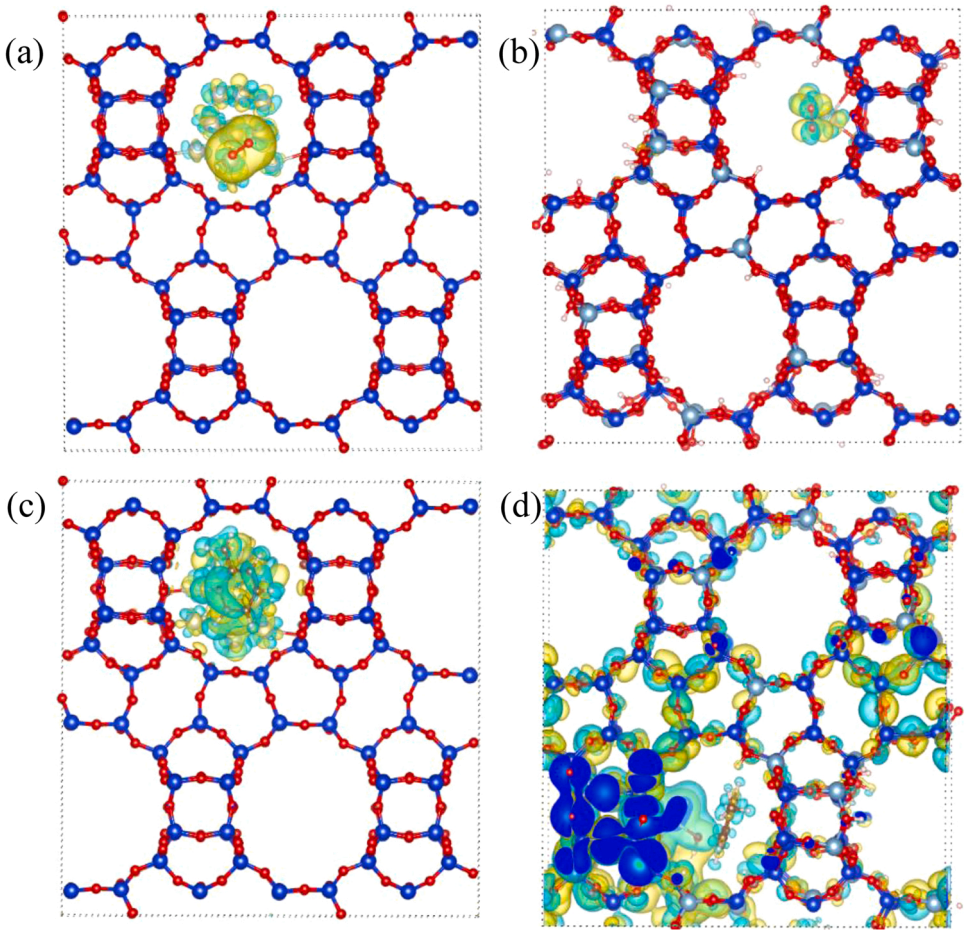

Fig. 10. Electron density difference of O_2 adsorbed in (a) Pt_{13}/BEA and (b) Pt/BEA-Al; electron density difference for toluene adsorbed in (c) Pt_{13}/BEA and (d) Pt/BEA-Al.

Conceptualization, Data acquisition, Data analysis. **Zhilin Zhang:** Data acquisition, Data analysis. **Yingjie Wang:** Data analysis. **Ying Ma:** Data analysis. **Tingting Pan:** Data acquisition. **Qian Zhao:** Data analysis **Yulong Shan:** Data analysis. **Xiaoyan Shi:** Data analysis. **Jinzhu Ma:** Data analysis. **Hong He:** Writing – review & editing, Supervision, Project administration.

Declaration of Competing Interest

The authors declare that they have no known competing financial interests or personal relationships that could have appeared to influence the work reported in this paper.

Data availability

Data will be made available on request.

Acknowledgments

This work was financially supported by the National Key R&D Program of China (2022YFC3702804), the National Natural Science Foundation of China (No. 21936005, 52022104, and 22106170), the Special Projects of Science and Technology of Hebei Province (22293701Z), and the Chinese Academy of Sciences (JCPYJJ-22053). We thank the 1W1B-XAFS experimental station in Beijing Synchrotron Radiation Facility (BSRF) for providing the beam time.

Appendix A. Supporting information

Supplementary data associated with this article can be found in the online version at doi:10.1016/j.apcatb.2023.122811.

References

[1] Y. Ma, L. Wang, J. Ma, H. Wang, C. Zhang, H. Deng, H. He, Investigation into the enhanced catalytic oxidation of o-Xylene over MOF-derived Co_3O_4 with different shapes: the role of surface twofold-coordinate lattice oxygen (O_{2f}), ACS Catal. 11 (2021) 6614–6625.

[2] H. Deng, Y. Lu, T. Pan, L. Wang, C. Zhang, H. He, Metals incorporated into OMS-2 lattice create flexible catalysts with highly efficient activity in VOCs combustion, Appl. Catal. B Environ. 320 (2023), 121955.

[3] T. He, X.J. Kong, Z.X. Bian, Y.Z. Zhang, G.R. Si, L.H. Xie, X.Q. Wu, H. Huang, Z. Chang, X.H. Bu, M.J. Zaworotko, Z.R. Nie, J.R. Li, Trace removal of benzene vapour using double-walled metal-dipyrazolate frameworks, Nat. Mater. 21 (2022) 689–695.

[4] C. Dong, J.J. Yang, L.H. Xie, G. Cui, W.H. Fang, J.R. Li, Catalytic ozone decomposition and adsorptive VOCs removal in bimetallic metal-organic frameworks, Nat. Commun. 13 (2022) 4991.

[5] Y. Ma, L. Wang, J. Ma, F. Liu, H. Einaga, H. He, Improved and reduced performance of Cu- and Ni-substituted Co_3O_4 catalysts with varying Co_{Oh}/Co_{Td} and Co^{3+}/Co^{2+} ratios for the complete catalytic oxidation of VOCs, Environ. Sci. Technol. 56 (2022) 9751–9761.

[6] C. Yang, G. Miao, Y. Pi, Q. Xia, J. Wu, Z. Li, J. Xiao, Abatement of various types of VOCs by adsorption/catalytic oxidation: a review, Chem. Eng. J. 370 (2019) 1128–1153.

[7] L. Wang, H. He, C. Zhang, Y. Wang, B. Zhang, Effects of precursors for manganese-loaded γ-Al_2O_3 catalysts on plasma-catalytic removal of o-xylene, Chem. Eng. J. 288 (2016) 406–413.

[8] H. Einaga, A. Ogata, Benzene oxidation with ozone over supported manganese oxide catalysts: effect of catalyst support and reaction conditions, J. Hazard. Mater. 164 (2009) 1236–1241.

[9] Q. Yang, Q. Li, L. Li, Y. Peng, D. Wang, Y. Ma, J. Li, Synthesis of alpha-MnO_2-like rod catalyst using YMn_2O_5 A-site sacrificial strategy for efficient benzene oxidation, J. Hazard. Mater. 403 (2021), 123811.

[10] C. He, J. Cheng, X. Zhang, M. Douthwaite, S. Pattisson, Z. Hao, Recent advances in the catalytic oxidation of volatile organic compounds: a review based on pollutant sorts and sources, Chem. Rev. 119 (2019) 4471–4568.

[11] A. Bhat, A.J. Hill, G.B. Fisher, J.W. Schwank, Improving the thermal stability and n-butanol oxidation activity of Ag-TiO_2 catalysts by controlling the catalyst architecture and reaction conditions, Appl. Catal. B Environ. 297 (2021), 120476.

[12] L. Yang, Q. Liu, R. Han, K. Fu, Y. Su, Y. Zheng, X. Wu, C. Song, N. Ji, X. Lu, D. Ma, Confinement and synergy effect of bimetallic Pt-Mn nanoparticles encapsulated in ZSM-5 zeolite with superior performance for acetone catalytic oxidation, Appl. Catal. B Environ. 309 (2022), 121224.

[13] H. Deng, T. Pan, Y. Zhang, L. Wang, Q. Wu, J. Ma, W. Shan, H. He, Adsorptive removal of toluene and dichloromethane from humid exhaust on MFI, BEA and FAU zeolites: an experimental and theoretical study, Chem. Eng. J. 394 (2020), 124986.

[14] H.P. Winoto, Z.A. Fikri, J.M. Ha, Y.K. Park, H. Lee, D.J. Suh, J. Jae, Heteropolyacid supported on Zr-Beta zeolite as an active catalyst for one-pot transformation of furfural to γ-valerolactone, Appl. Catal. B Environ. 241 (2019) 588–597.

[15] S. Zou, M. Zhang, S. Mo, H. Cheng, M. Fu, P. Chen, L. Chen, W. Shi, D. Ye, Catalytic performance of toluene combustion over Pt nanoparticles supported on pore-modified macro-meso-microporous zeolite foam, Nanomater 10 (2019) 1–16.

[16] C. Chen, F. Chen, L. Zhang, S. Pan, C. Bian, X. Zheng, X. Meng, F.S. Xiao, Importance of platinum particle size for complete oxidation of toluene over Pt/ZSM-5 catalysts, Chem. Commun. 51 (2015) 5936–5938.

[17] C. Chen, Q. Wu, F. Chen, L. Zhang, S. Pan, C. Bian, X. Zheng, X. Meng, F. Xiao, Aluminium-rich Beta zeolite-supported platinum nanoparticles for the low-temperature catalytic removal of toluene, J. Mater. Chem. A 3 (2015) 5556–5562.

[18] D. Cheng, X. Meng, Recent advances of Beta zeolite in the volatile organic compounds (VOCs) elimination by the catalytic oxidations, Chem. Res. Chin. Univ. 38 (2022) 716–722.

[19] Y. Shi, Z. Li, J. Wang, R. Zhou, Synergistic effect of Pt/Ce and USY zeolite in Pt-based catalysts with high activity for VOCs degradation, Appl. Catal. B Environ. 286 (2021), 119936.

[20] Y. Yang, G. Wang, P. Zheng, F. Dang, J. Han, Carbon deposits during catalytic combustion of toluene on Pd–Pt-based catalysts, Catal. Sci. Technol. 10 (2020) 2452–2461.

[21] P. Dege, L. Pinard, P. Magnoux, M. Guisnet, Catalytic oxidation of volatile organic compounds II. Influence of the physicochemical characteristics of Pd/HFAU catalysts on the oxidation of o-xylene, Appl. Catal. B Environ. 27 (2000) 17–26.

[22] A.W. Petrov, D. Ferri, F. Krumeich, M. Nachtegaal, J.A. van Bokhoven, O. Krocher, Stable complete methane oxidation over palladium based zeolite catalysts, Nat. Commun. 9 (2018) 2545.

[23] J.E. Samad, J. Blanchard, C. Sayag, C. Louis, J.R. Regalbuto, The controlled synthesis of metal-acid bifunctional catalysts: the effect of metal:acid ratio and metal-acid proximity in Pt silica-alumina catalysts for n-heptane isomerization, J. Catal. 342 (2016) 203–212.

[24] M. Kraus, U. Trommler, F. Holzer, F.D. Kopinke, U. Roland, Competing adsorption of toluene and water on various zeolites, Chem. Eng. J. 351 (2018) 356–363.

[25] Y. Jiang, L. Zhang, Y. Xie, S. Han, Q. Zhu, X. Meng, F. Xiao, Enhanced catalytic activity in propene oxidation over NaZSM-5 zeolite-supported Pt nanoparticles by increasing the zeolite Si/Al ratio, Catal. Today 355 (2020) 476–481.

[26] S.F. Rastegar, G. Sadovska, R. Pilar, J. Moravkova, D. Kaucky, L. Brabec, J. Pastvova, P. Sazama, Analysis of decisive structural parameters of zeolites for alkylation of benzene with ethylene, Appl. Catal. A Gen. 591 (2020), 117379.

[27] C. Auepattana-aumrung, K. Suriye, B. Jongsomjit, J. Panpranot, P. Praserthdam, Inhibition effect of Na^+ form in ZSM-5 zeolite on hydrogen transfer reaction via 1-butene cracking, Catal. Today 358 (2020) 237–245.

[28] Y. Du, G. Xiao, Z. Guo, B. Lin, M. Fu, D. Ye, Y. Hu, A high-performance and stable Cu/Beta for adsorption-catalytic oxidation in-situ destruction of low concentration toluene, Sci. Total Environ. 833 (2022), 155288.

[29] T.D. Kuhne, M. Iannuzzi, M. Del Ben, V.V. Rybkin, P. Seewald, F. Stein, T. Laino, R. Z. Khaliullin, O. Schutt, F. Schiffmann, D. Golze, J. Wilhelm, S. Kuhne, M.H. Bani Hashemian, V. Weber, U. Borstnik, M. Taillefumier, A.S. Jakobovits, A. Lazzaro, H. Pabst, T. Muller, R. Schade, M. Guidon, S. Andermatt, N. Holmberg, G. K. Schenter, A. Hehn, A. Bussy, F. Belleflamme, G. Tabacchi, A. Gloss, M. Lass, I. Bethune, C.J. Mundy, C. Plessl, M. Watkins, J. VandeVondele, M. Krack, J. Hutter, CP2K: an electronic structure and molecular dynamics software package - quickstep: efficient and accurate electronic structure calculations, J. Chem. Phys. 152 (2020) 47.

[30] M. Krack, Pseudopotentials for H to Kr optimized for gradient-corrected exchange-correlation functionals, Theor. Chem. Acc. 114 (2005) 145–152.

[31] S. Grimme, J. Antony, S. Ehrlich, H. Krieg, A consistent and accurate ab initio parametrization of density functional dispersion correction (DFT-D) for the 94 elements H-Pu, J. Chem. Phys. 132 (2010) 19.

[32] C. Chen, J. Zhu, F. Chen, X. Meng, X. Zheng, X. Gao, F.-S. Xiao, Enhanced performance in catalytic combustion of toluene over mesoporous Beta zeolite-supported platinum catalyst, Appl. Catal. B: Environ. 140-141 (2013) 199–205.

[33] D. Li, Y. Zheng, X.Y. Wang, Effect of phosphoric acid on catalytic combustion of trichloroethylene over Pt/P-MCM-41, Appl. Catal. A Gen. 340 (2008) 33–41.

[34] R. Li, T. Xue, Z. Li, Q. Wang, Hierarchical structure ZSM-5/SBA-15 composite with improved hydrophobicity for adsorption-desorption behavior of toluene, Chem. Eng. J. 392 (2020), 124861.

[35] B. Wu, B. Chen, X. Zhu, L. Yu, C. Shi, Lower loading of Pt on hydrophobic TS-1 zeolite: a high-efficiency catalyst for benzene oxidation at low temperature, Catal. Today 355 (2020) 512–517.

[36] L. Zhang, L. Chen, Y. Li, Y. Peng, F. Chen, L. Wang, C. Zhang, X. Meng, H. He, F. Xiao, Complete oxidation of formaldehyde at room temperature over an Al-rich Beta zeolite supported platinum catalyst, Appl. Catal. B Environ. 219 (2017) 200–208.

[37] S. Huang, D. Yang, Q. Tang, W. Deng, L. Zhang, Z. Jia, Z. Tian, Q. Gao, L. Guo, Pt-loaded ellipsoidal nanozeolite as an active catalyst for toluene catalytic combustion, Microporous Mesoporous Mater 305 (2020), 110292.

[38] T. Toyao, S. Kayamori, Z. Maeno, S.M.A.H. Siddiki, Ki Shimizu, Heterogeneous Pt and MoO_x Co-loaded TiO_2 catalysts for low-temperature CO_2 hydrogenation to form CH_3OH, ACS Catal. 9 (2019) 8187–8196.

[39] Z. Jiang, M. Tian, M. Jing, S. Chai, Y. Jian, C. Chen, M. Douthwaite, L. Zheng, M. Ma, W. Song, J. Liu, J. Yu, C. He, Modulating the electronic metal-support interactions in single-atom Pt_1 -CuO catalyst for boosting acetone oxidation, Angew. Chem. Int. Ed. 61 (2022), e202200763.

[40] K. Ding, A. Gulec, A.M. Johnson, N.M. Schweitzer, G.D. Stucky, L.D. Marks, P. C. Stair, Identification of active sites in CO oxidation and water-gas shift over supported Pt catalysts, Science 350 (2015) 189–192.

[41] K. Chakarova, M. Mihaylov, K. Hadjiivanov, FTIR spectroscopic study of CO adsorption on Pt–H–ZSM-5, Microporous Mesoporous Mater 81 (2005) 305–312.

[42] L. Shi, X. Song, G. Liu, H. Guo, Effect of catalyst preparation on hydroisomerization of n-heptane over Pt/Silicalite-1, Catal. Lett. 147 (2017) 2549–2557.

[43] L.W. Ho, C.P. Hwang, J.F. Lee, I. Wang, C.T. Yeh, Reduction of platinum dispersed on dealuminated Beta zeolite, J. Mol. Catal. A-Chem. 136 (1998) 293–299.

[44] T.M. Lardinois, J.S. Bates, H.H. Lippie, C.K. Russell, J.T. Miller, H.M. Meyer, K. A. Unocic, V. Prikhodko, X. Wei, C.K. Lambert, A.B. Getsoian, R. Gounder, Structural interconversion between agglomerated palladium domains and mononuclear Pd(II) cations in chabazite zeolites, Chem. Mater. 33 (2021) 1698–1713.

[45] Z. Guo, X. Li, S. Hu, G. Ye, X. Zhou, M.O. Coppens, Understanding the role of internal diffusion barriers in Pt/Beta zeolite catalyzed isomerization of n-heptane, Angew. Chem. Int. Ed. 59 (2020) 1548–1551.

[46] R. Roldan, A. Beale, M. Sanchezsanchez, F. Romerosalguero, C. Jimenezsanchidrian, J. Gomez, G. Sankar, Effect of the impregnation order on the nature of metal particles of bi-functional Pt/Pd-supported zeolite Beta materials and on their catalytic activity for the hydroisomerization of alkanes, J. Catal. 254 (2008) 12–26.

[47] C. Chizallet, Toward the atomic scale simulation of intricate acidic aluminosilicate catalysts, ACS Catal. 10 (2020) 5579–5601.

[48] R. Liu, S. Zeng, T. Sun, S. Xu, Z. Yu, Y. Wei, Z. Liu, Selective removal of acid sites in mordenite zeolite by trimethylchlorosilane silylation to improve dimethyl ether carbonylation stability, ACS Catal. 12 (2022) 4491–4500.

[49] Y. Wang, X. Shi, Z. Liu, Y. Shan, W. Shi, Y. Yu, H. He, The study of Pd-SSZ-13 as low-temperature passive NO adsorber materials: high dispersal of Pd in small-pore CHA zeolites by thermal treatment, Appl. Catal. B Environ. 324 (2023), 122254.

[50] M. Popova, A. Szegedi, M. Oykova, H. Lazarova, N. Koseva, M.R. Mihalyi, D. Karashanova, Y. Mitrev, P. Shestakova, Hydrodemethoxylation/dealkylation on bifunctional nanosized zeolite beta, Molecules 26 (2021) 7694.

[51] Z. Yu, A. Zheng, Q. Wang, L. Chen, J. Xu, J.P. Amoureux, F. Deng, Insights into the dealumination of zeolite HY revealed by sensitivity-enhanced ^{27}Al DQ-MAS NMR spectroscopy at high field, Angew. Chem. Int. Ed. 49 (2010) 8657–8661.

[52] M. Haouas, F. Taulelle, C. Martineau, Recent advances in application of ^{27}Al NMR spectroscopy to materials science, Prog. Nucl. Magn. Reson. Spectrosc. 94- 95 (2016) 11–36.

[53] P.S.F. Mendes, A.-L. Taleb, A.-S. Gay, A. Daudin, C. Bouchy, J.M. Silva, M. F. Ribeiro, Nanoscale insights into Pt-impregnated mixtures of zeolites, J. Mater. Chem. A 5 (2017) 16822–16833.

[54] A. Penkova, S. Dzwigaj, R. Kefirov, K. Hadjiivanov, M. Che, Effect of the preparation method on the state of nickel ions in BEA zeolites. A study by Fourier transform infrared spectroscopy of adsorbed CO and NO, temperature-programmed reduction, and X-ray diffraction, J. Phys. Chem. C. 111 (2007) 8623–8631.

[55] J. Li, W. Zhang, C. Li, H. Xiao, C. He, Insight into the catalytic performance and reaction routes for toluene total oxidation over facilely prepared Mn-Cu bimetallic oxide catalysts, Appl. Surf. Sci. 550 (2021), 149179.

[56] J. Cejka, A. Vondrova, B. Wichterlova, H.G. Jerschkewitz, G. Lischke, E. Schreier, The effect of extra-framework aluminum in dealuminated ZSM-5 zeolites on the transformation of aromatic hydrocarbons, Collect. Czech. Chem. Commun. 60 (1995) 412–420.

[57] Z. Zhang, G. He, Y. Li, C. Zhang, J. Ma, H. He, Effect of hydroxyl groups on metal anchoring and formaldehyde oxidation performance of Pt/Al_2O_3, Environ. Sci. Technol. 56 (2022) 10916–10924.

[58] H. Zhu, Pd/CeO_2-TiO_2 catalyst for CO oxidation at low temperature: a TPR study with H_2 and CO as reducing agents, J. Catal. 225 (2004) 267–277.

[59] J.A. Santana, DFT calculations of the adsorption states of O(2) on OH/H(2)O-Covered Pt(111), Electrocatalysis 11 (2020) 612–617.

[60] W. Yang, Y. Peng, Y. Wang, Y. Wang, H. Liu, Za Su, W. Yang, J. Chen, W. Si, J. Li, Controllable redox-induced in-situ growth of MnO_2 over Mn_2O_3 for toluene oxidation: active heterostructure interfaces, Appl. Catal. B Environ. 278 (2020), 119279.

[61] Q. Zhang, W. Su, P. Ning, X. Liu, H. Wang, J. Hu, Catalytic performance and mechanistic study of toluene combustion over the Pt-Pd-HMS catalyst, Chem. Eng. Sci. 205 (2019) 230–237.

[62] P. Chen, W. Cui, H. Wang, Xa Dong, J. Li, Y. Sun, Y. Zhou, Y. Zhang, F. Dong, The importance of intermediates ring-opening in preventing photocatalyst deactivation during toluene decomposition, Appl. Catal. B Environ. 272 (2020), 118977.
[63] K. Zhang, L. Dai, Y. Liu, J. Deng, L. Jing, K. Zhang, Z. Hou, X. Zhang, J. Wang, Y. Feng, Y. Zhang, H. Dai, Insights into the active sites of chlorine-resistant Pt-based bimetallic catalysts for benzene oxidation, Appl. Catal. B Environ. 279 (2020), 119372.
[64] J. Chen, Y. Yang, S. Zhao, F. Bi, L. Song, N. Liu, J. Xu, Y. Wang, X. Zhang, Stable black phosphorus encapsulation in porous mesh-like UiO-66 promoted charge transfer for photocatalytic oxidation of toluene and o-dichlorobenzene: performance, degradation pathway, and mechanism, ACS Catal. 12 (2022) 8069–8081.
[65] M. Navlani García, M. Martis, D. Lozano Castelló, D. Cazorla Amorós, K. Mori, H. Yamashita, Investigation of Pd nanoparticles supported on zeolites for hydrogen production from formic acid dehydrogenation, Catal. Sci. Technol. 5 (2015) 364–371.